Was the observed pre-seismic total electron content enhancement a true precursor of the 2011 Tohoku-Oki Earthquake?

R. Ikuta[1], T. Hisada[1], G. Karakama[2], O. Kuwano[3]

[1]Faculty of Science, Shizuoka University, Japan

[2]Graduate School of Environmental Studies, Nagoya University, Japan

[3]JAMSTEC, Japan

Abstract

Here we test the precursory enhancement in ionospheric total electron content (TEC) measured by GNSS leading up to the 2011 Mw9.0 Tohoku-Oki Earthquake. We verify the frequency of this TEC enhancement via analysis of a two-month vertical TEC (VTEC) time series that included the Tohoku-Oki Earthquake using the procedure, based on Akaike's information criterion, and threshold of Heki and Enomoto [2015].The averaged occurrence rate of the TEC enhancement is much larger than that reported by Heki and Enomoto [2015] when all of the visible GPS satellites at a given station are taken into account. We cannot rule out the possibility that the pre-seismic VTEC changes before the great earthquakes that were reported by Heki and Enomoto [2015] are just a product of chance. Furthermore, we analyze the spatial distribution of the pre-seismic TEC enhancement and co-seismic TEC depletion for the Tohoku-Oki Earthquake. We observe significant post-seismic depletion that lasted at least 2 h after the earthquake and extended at least 500 km from the center of the large-slip area. The spatial distribution of this post-seismic depletion appears to be independent of the pre-seismic enhancement. The enhancement reported by Heki [2011] before the Tohoku-Oki Earthquake may therefore be

an apparent phenomenon related to the combined effects of a largescale traveling ionosphere disturbance and co-seismic ionospheric disturbance.

1. Introduction

Precursory enhancement of the ionospheric total electron content (TEC) within a few tens of minutes before large earthquakes has been reported by Heki [2011] and numerous Global Navigation Satellite System (GNSS) TEC observational studies (e.g., Heki and Enomoto, 2013; Heki and Enomoto, 2015; He and Heki, 2016, 2017, 2018). Heki [2011] extracted the TEC enhancement prior to the 2011 Tohoku-Oki Earthquake using a reference curve to model the slant TEC (STEC) time series, with the departure from the reference curve defining the TEC anomaly in the focal area. He excluded a 48-min time window surrounding the mainshock (from 34 min before to 14 min after the mainshock) from the STEC time series to deduce the reference curve, and showed that the residual STEC began to increase 40 min before the earthquake, returning to the normal state when the post-seismic acoustic wave reached the ionosphere [Heki, 2011]. However, this approach has received criticism (e.g., Kamogawa and Kakinami, 2013; Masci et al., 2015). Kamogawa and Kakinami [2013] attributed the TEC enhancement reported by Heki [2011] to an artifact caused by the combined effects of TEC disturbances under active geomagnetic conditions and an ionospheric hole generated by a tsunami. Heki and Enomoto [2013] revisited the data to address this criticism, and claimed that the tsunami did not make an ionospheric hole since their pre-seismic increase in the vertical TEC (VTEC) was comparable to the post-seismic decrease. They suggested that the post-seismic decrease was due to the recovery from the precursory TEC enhancement, rather than a post-seismic tsunamigenic hole [Heki and Enomoto, 2013]. This interpretation justifies the exclusion of the time window immediately surrounding the mainshock, for which the end time is generally set at 20 min after the mainshock, in deducing the reference VTEC curves in subsequent studies (e.g. He and Heki, 2016, 2017, 2018). However, He and Heki [2017] also considered the possibility of a post-seismic hole by studying the pre-seismic enhancement of Mw 7–8 earthquakes using the reference curves. They claimed that these TEC depletions should be spatially limited above the focal area, even if the post-seismic holes persist for a while, such that excluding the ±30-min time window surrounding the earthquake is enough to avoid these effects because the ionospheric penetration point (IPP) along the line of sight (LOS) between a station and satellite can pass through the area within this period [He and Heki, 2017]. In addition to these rebuttals, Heki and Enomoto [2015] detected a positive break in the TEC time series (sudden increase in the TEC rate) without using reference curves before five huge earthquakes based on Akaike's information criterion (AIC). They claimed that whether this positive break is space weather origin or not could be judged stochastically, even though the propagation of the positive break resembles a large-scale traveling ionospheric disturbance (LSTID) and there were active geomagnetic conditions during the period surrounding the 2011 Tohoku-Oki Earthquake [Heki and Enomoto, 2015]. They detected positive breaks for five of the eight analyzed Mw 8.2–9.2 earthquakes, and showed that the frequency of the breaks exceeding their TEC unit (TECU) threshold (3.0 TECU/h) was below 1/10, which was the averaged frequency over the three-week period surrounding the 2011 Tohoku-Oki Earthquake. They then assumed a random occurrence of these breaks with a probability of 1/10 per hour, and determined that the detection probability of such breaks during the 1.5-h period before the five earthquakes would be $(1.5 \times 1/10)^5$, which is too small to be considered a fortuity. However, their sampling approach would have underestimated the occurrence rate if the TEC enhancement varied between different satellites, even though they only used one satellite to demonstrate the occurrence rate of the break.

Here we first test the occurrence rate of the TEC break using all of the visible satellites during a 61-day period surrounding the 2011 Tohoku-Oki Earthquake. We then observe the spatiotemporal pre-seismic and co-seismic VTEC variations at the time of the Tohoku-Oki Earthquake to clarify the spatial relationship between the pre-seismic enhancement and post-seismic depletion.

2. TEC data processing

We calculated the VTEC time series from the L1 and L2 carrier phases of the global positioning system (GPS) signal for each GNSS station–satellite pair of the GNSS Earth Observation Network (GEONET) by implementing the following procedures.

2-1. Convert the geometry-free linear combination (L4) into the VTEC deviation (ΔTEC)

We first obtained the phases of the L1 and L2 signals to calculate the carrier phase geometry-free combination (L4). We removed the cycle slips from L4 based on its jump, and then shifted L4 to fit the geometry-free linear combination between the C1 and P2 codes to remove the phase ambiguities. This shifted L4 was multiplied by a constant $\frac{10^{-16} f_1^2 f_2^2}{40.308(f_1^2 - f_2^2)}$, where f_1 and f_2 are the dominant frequencies of the L1 and L2 signals, respectively, to obtain the VTEC deviation (ΔTEC). ΔTEC is measured in TECU, where 1 TECU is equivalent to 10^{16} electrons m^{-2}, which also corresponds to 0.162 m and 0.2675 m of the L1 and L2 signal delays, respectively.

The inter-frequency biases (IFBs) of the stations and differential code biases (DCBs) of the satellites are both included in the ΔTEC data. We corrected for these biases to obtain meaningful slant TEC (STEC) values as follows:

$$STEC_{ij}(t) = \Delta TEC_{ij}(t) - DCB_j - IFB_i, \tag{1}$$

where t is the time, and DCB_j and IFB_i correspond to the j-th satellite and i-th receiver, respectively. STEC was then converted to VTEC as follows:

$$VTEC_{ij}(t) = STEC_{ij}(t)\, cos\psi_{ij}(t), \tag{2}$$

where ψ_{ij} is the incident angle of the signal penetrating the ionosphere at the IPP. The satellite's DCBs between C1 and P2 were calculated from the P1–C1 and P1–P2 code biases provided by the University of Bern (ftp.unibe.ch). The receiver's IFBs between C1 and P2 were provided by the Electronic Navigation Research Institute (ENRI) [Sakai, 2005].

2-2. TEC break detection

Heki and Enomoto [2015] evaluated the occurrence rate of the TEC enhancement in the VTEC time series using only one station–satellite pair; we followed their methodology here. A moving window was adopted that fit a pair of lines to the VTEC curve, with the linear break between the two lines set at the middle of the window. The significance of the break on the fit was determined by calculating the difference of AIC value between the two lines with break and a single line that was fit to the entire VTEC curve in the window. This difference is denoted as –ΔAIC; a pair of lines is judged to provide a better fit to the VTEC curve than a single line when –ΔAIC is positive. The TEC enhancement was then evaluated by comparing the increase in slope of the latter line to that of the former line when –ΔAIC was positive. The break was regarded as a "significant positive break" when the increase in slope between the two linear fits exceeded a certain threshold. Here we expanded the approach of Heki and Enomoto [2015] by applying this procedure to all of the visible satellites from GNSS station 3009 instead of using only a single satellite–station pair (They used only PRN15). This approach is more reasonable to simulate the situation that a precursor seeker can choose any one of all visible satellites when they look for a positive break prior to a great earthquake. We adopted a ±30-min time window and regard an increase that was larger than 3.0 TECU/h (absolute) and 75% of the original rate (relative) as a significant positive break, following Heki and Enomoto [2015].

3. Results: Spatiotemporal distribution of positive breaks

Figure 1 shows the VTEC time series for the three-week period surrounding the 2011 Tohoku-Oki Earthquake, using the same dataset as Heki and Enomoto [2015] (satellite PRN15 and GNSS station 3009); the time series looks similar to that in figure 6 of Heki and Enomoto [2015]. Positive breaks are detected seven times (red dots in Figure 1), including the pre-seismic break before the Tohoku-Oki Earthquake, as observed by Heki and Enomoto [2015]. The two breaks just after the Tohoku Oki Earthquake are not taken into account here (gray dots in Figure 1), as they are mentioned by Heki and Enomoto [2015].

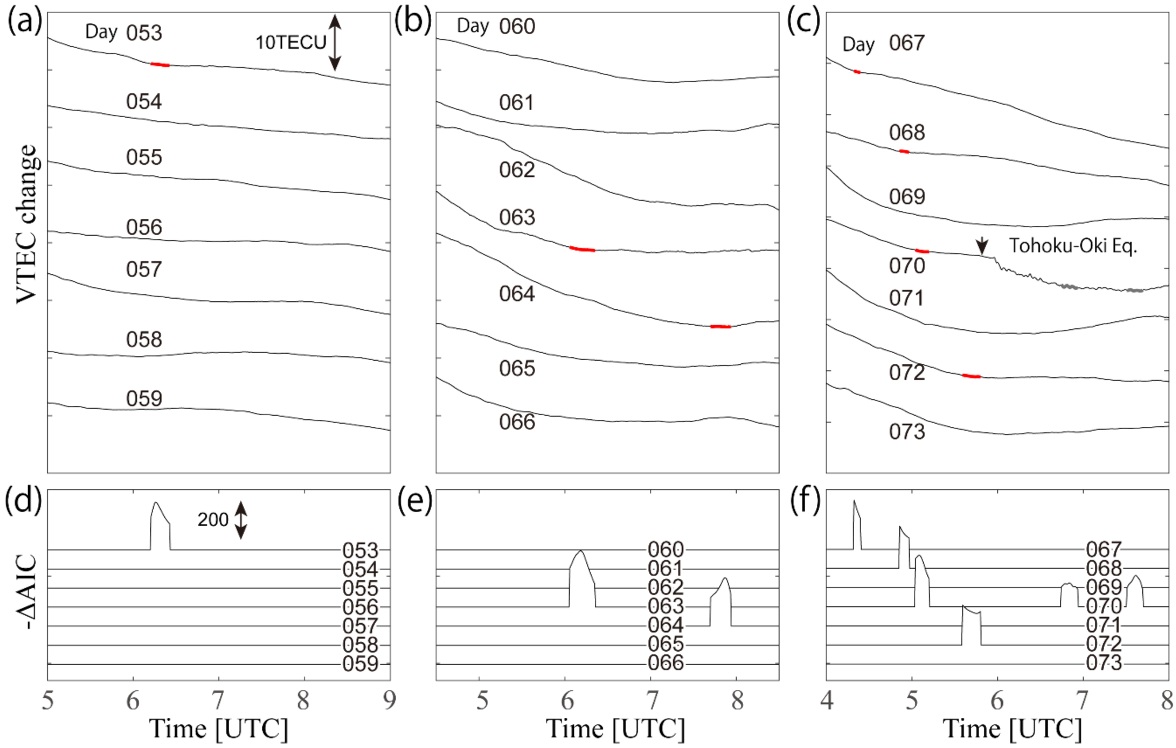

Figure 1. VTEC time series for the three-week period surrounding the 2011 Tohoku-Oki Earthquake (same dataset as used in making figure 6 of Heki and Enomoto [2015]) for the same satellite (PRN15)–GNSS station (3009) pair. (a–c) VTEC time series. The red sections represent significant positive breaks (±30-min time window) that exceed 3 TECU/h and 75% of the original rate. The gray sections shortly after the Tohoku-Oki Earthquake also represent positive breaks but not counted considering post seismic variation. (d–f) –ΔAIC calculated for (a)–(c), respectively.

We applied this analysis to the 61-day VTEC time series from 9 February (DOY40) to 10 April 2011 (DOY100). The positive break rate should have been accurately evaluated by Heki and Enomoto [2015] if it was simultaneously observed by all of the visible satellites. However, their positive break rate, which was evaluated using only one satellite, would be an underestimate if it was independently observed by each satellite because they would have missed positive breaks that occurred at satellites other than PRN15 at different times in the study period.

Figure 2a shows the number of detected significant positive breaks during the daytime

(12:00–17:00 local time (LT); 03:00–08:00 UTC) for each day during the 61-day period. The breaks were calculated using all of the visible satellites with an elevation angle higher than 25°. If a period where the slope exceeds the threshold overlapped with a period from one or more other satellites, then these periods were regarded as one event. A total of 198 positive break events were detected within the 305-h observation period, resulting in an averaged occurrence rate of 0.65 times per hour. Approximately 36% of the breaks were detected simultaneously by multiple satellites, with the remaining 64% detected by one satellite (Figure 2b). The positive break 40 min before the Tohoku-Oki Earthquake was detected by two satellites (PRN15 and 26).

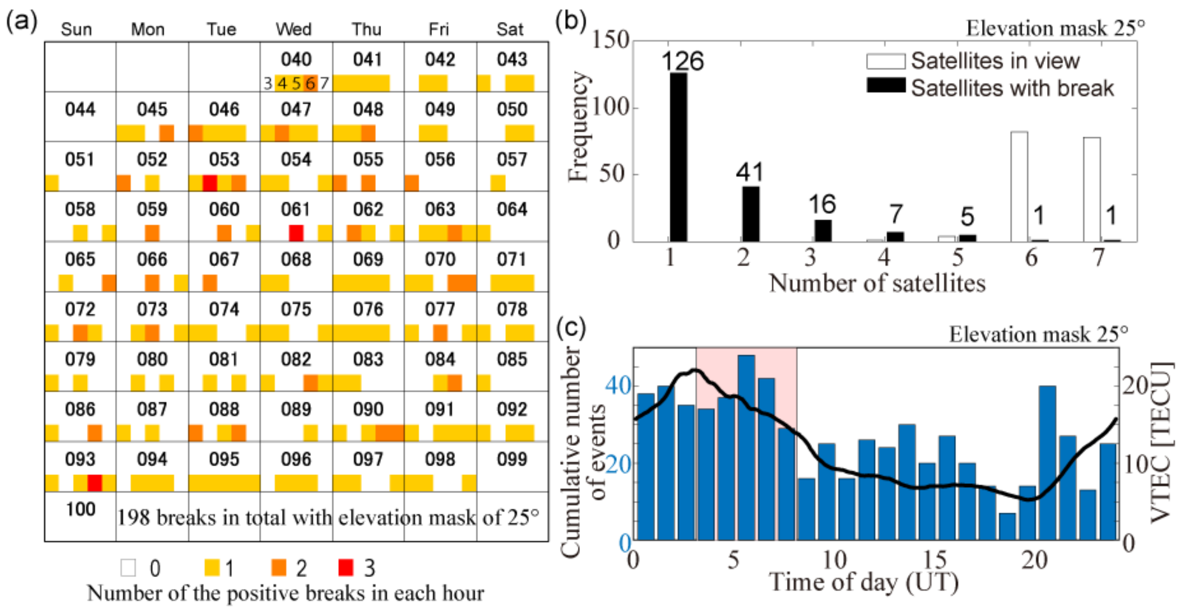

Figure 2. Frequency of positive TEC breaks during the 61-day period. (a) Number of positive breaks in calendar time, with an elevation mask angle of 25°. The number at the top of each cell is the day of year. The small numbers in the day 040 cell denote the five 1-h periods, which span from 03:00 to 08:00 UTC. The colors indicate the number of detected breaks in each 1-h period. (b) Frequency of satellites in view that detected a

positive break, with an elevation mask angle of 25°. The white bars show the number of satellites in view when a positive break is detected. The black bars show the number of satellites that simultaneously detected a break. (c) Frequency of positive TEC breaks as a function of time of day during the 61-day period. The blue bars indicate the cumulative number of positive TEC break events that were detected during each hour. The solid line shows the 61-day-averaged VTEC time series. The shaded magenta region highlights the time of day that was the focus of the analysis in (a) and (b) (03:00–08:00 UTC).

The diurnal variations in Figure 2c show that the occurrence rate of the positive break is higher in the daytime (09:00–17:00 LT; 00:00–08:00 UTC) and early morning (05:00–07:00 LT; 20:00–22:00 UTC). Positive breaks are detected about three times more frequently during the daytime than in the predawn hours (02:00–05:00 LT (17:00–20:00 UTC), which is explained by variations in the background VTEC level. The high rate of break detection in the early morning is explained by TEC enhancement at dawn.

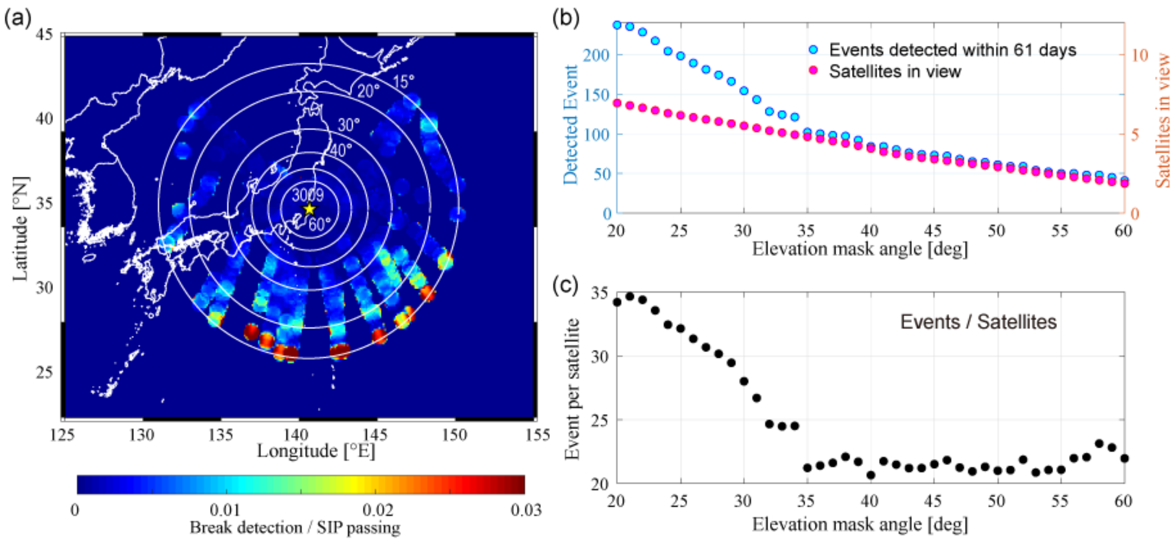

Figure 3. (a) Number of detected events and satellites in view against various elevation

mask angles. (b) Number of events detected within the 61-day period (cyan) and average number of satellites in view (magenta) for a range of elevation mask angles. (c) Number of detected positive break events divided by the number of satellites in view. The expected number of events per satellite is approximately constant when the elevation mask angle is larger than 35°.

The positive break detection is also highly dependent on the LOS configuration. Figure 3a shows the spatial distribution of the detection rate of breaks at sub-ionospheric points (SIPs), which is calculated by dividing the number of detected positive breaks by the SIP density. More positive breaks tend to be detected when the satellites are at a lower elevation angle. The detection rate is very high when the elevation is below 20°, especially in the southern sky. Figure 3b shows the relationship between the elevation mask and number of detected TEC breaks. The number of detected events is proportional to the number of satellites in view when the elevation mask angle is larger than 35°. However, the number of detected events increases much more rapidly than the number of satellites in view when the elevation mask angle is less than 35°. This trend should be due to unstable VTEC behavior in the low-angle LOS, as in this case the ray paths travel longer distances through the ionosphere. Each satellite detected an average of 21–22 breaks during the 61-day period when the elevation mask angle was larger than 35° (Figure 3c). This detection rate is similar to that in Heki and Enomoto [2015], where seven breaks were detected with satellite PRN15 over a 21-day period. A total of 98 positive TEC breaks are detected during the 61-day period when a 37° elevation mask angle is applied. Therefore, the occurrence rate of positive breaks is ~0.31 times per hour.

4. Discussion

The results of the statistical TEC evaluation illustrate that the significant positive breaks are observed much more often than reported by Heki and Enomoto [2015]. The average occurrence rate of the TEC positive breaks measured under the same conditions and threshold as those of Heki and Enomoto [2015], and the inclusion of all of the visible satellites, is 0.65 times per hour with a 25° elevation mask angle. This suggests that the pre-seismic TEC enhancement reported by Heki [2011] as being a precursory phenomenon may have been a product of chance.

Here we first evaluate the positive TEC breaks observed before the eight great earthquakes reported by Heki and Enomoto [2015] from a stochastic viewpoint. We then discuss the spatiotemporal VTEC distribution before and after the 2011 Tohoku-Oki Earthquake.

4-1. Stochastic evaluation of the pre-seismic breaks

Heki and Enomoto [2015] reported significant positive TEC breaks (exceeding the absolute 3.0 TECU/h and relative 75% threshold) before five Mw 8–9 earthquakes. We evaluate the probability of the case where the breaks are observed within 90 min before five of the eight events assuming a Poisson process. The probability of observing n events during a time period when μ events occur is expressed as follows:

$$f(n) = \frac{\mu^n}{n!} e^{-\mu}. \quad (3)$$

The average rate is 0.98 times per 90 min (μ = 0.98) when a 25° elevation mask angle is assumed, and the probability of observing at least one event during the time period is $1 - f(0) = 0.62$. The 25° elevation mask angle that is adopted in this evaluation is not too small, as the pre-seismic breaks that were extracted by Heki and Enomoto [2015] included breaks at very low elevation angles, such as 15° for the 2012 Mw 8.6 North Sumatra Earthquake.

This 62% probability indicates that a pre-seismic positive TEC break is expected for 62 of 100 earthquakes. The reported significant pre-seismic positive TEC breaks for five of the eight great earthquakes analyzed in Heki and Enomoto [2015] is reasonable from this probabilistic viewpoint.

4-2. Correspondence between the pre-seismic and post-seismic TEC changes

We next test the correspondence between the pre-seismic and post-seismic TEC changes reported by Heki and Enomoto [2013], where they proposed a temporal TEC variation model, with the post-seismic drop representing a recovery from the pre-seismic increase (as opposed to a net decrease). We follow their analysis by testing the correlation between the pre-seismic increase and post-seismic decrease in the VTEC time series around the source area. They modeled the VTEC time series from satellite PRN26 during the 3-h period surrounding the mainshock, which consisted of four lines connected by three breaks (Figure 4a; same as figure 3a in Heki and Enomoto [2013], but with the data analyzed using our procedure). They assumed that period A represented the background steady decrease in afternoon VTEC. Periods B and C correspond to the pre-seismic increase and co-seismic decrease, respectively. They compared the integrated changes during B and C relative to the trend during A, and found that the increase in B was comparable to the decrease in C, which led them to report no net post-seismic VTEC decrease [Heki and Enomoto, 2013]. However, their analysis only incorporated seven GNSS stations that were approximately aligned. We extend the GNSS station coverage to test the spatial distribution of the VTEC changes. Figure 4b shows the relationship between the two quantities for the broad GNSS station distribution shown in the map. This result indicates that the coincidence between the increase and decrease is not universal across the region, but rather limited to the stations selected by Heki and Enomoto [2013]. The spatial distributions of the increase and the decrease during periods B and C, respectively, exhibit notably different patterns (Figures 4c and 4d).

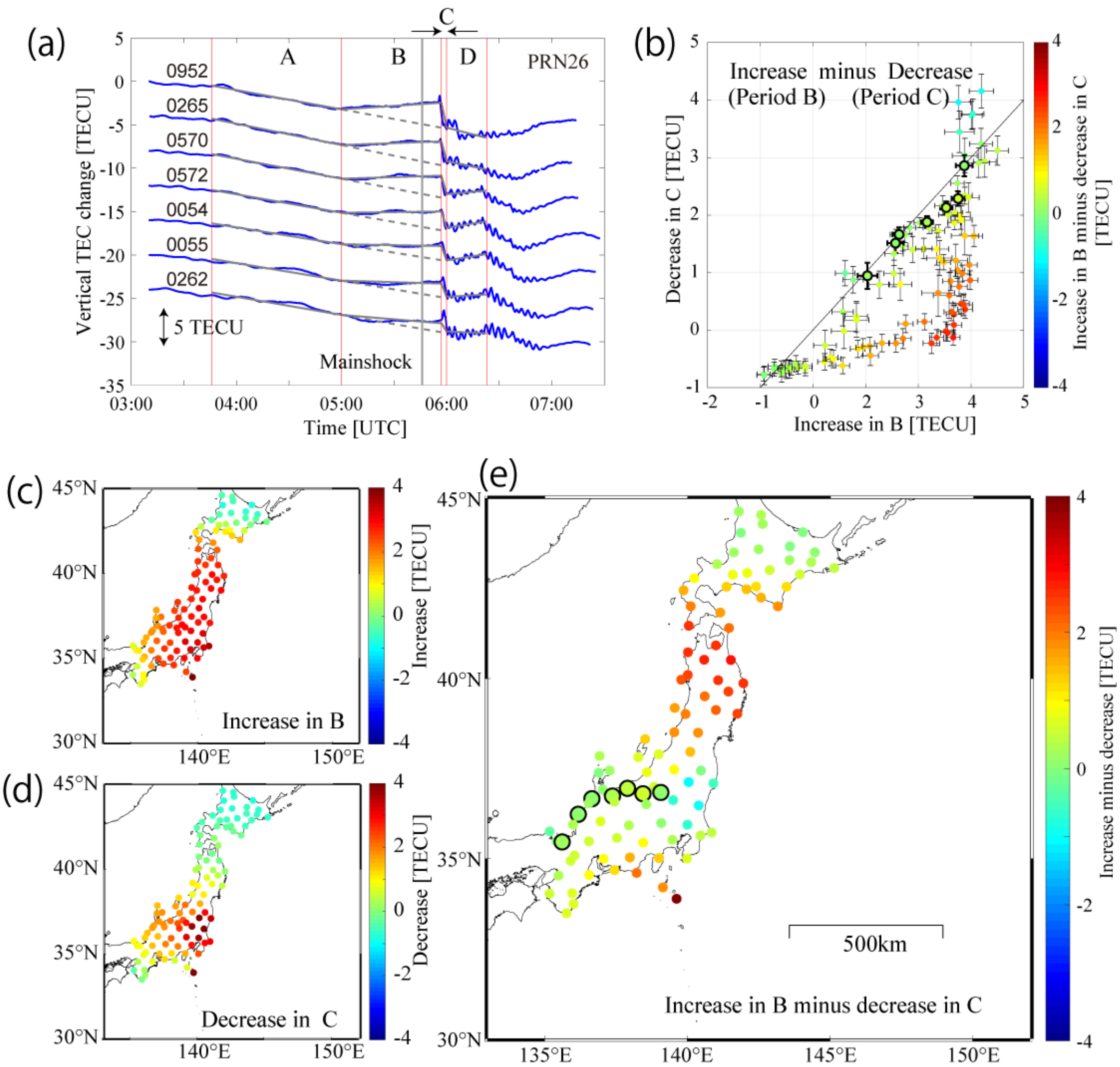

Figure 4. (a) VTEC time series from satellite PRN26 at seven GPS stations with various focal distances from the Tohoku-Oki Earthquake epicenter. The ~3-h period surrounding the mainshock (marked by the vertical gray line), spanning from 03:45 UTC (2 h before

the earthquake) to 06:25 UTC (~40 min after the earthquake), is divided into four segments (marked by the vertical red lines), which represent the (A) normal background, (B) precursory enhancement, (C) co-seismic drop, and (D) post-seismic periods, and a linear fit to each segment is determined (gray line segments). This figure is the same as figure 3a in Heki and Enomoto [2013], with the exception of the estimated VTEC time series used here. (b) Difference between the period B increase and period C decrease. The stations that were used by Heki and Enomoto [2013] are indicated by circles with thick lines. The error bars denote 1σ uncertainties. The observed difference is shown by the marker color. This figure is the same as figure 3c in Heki and Enomoto [2013], with the exception of the additional stations used in the analysis. (c) Spatial distribution of the degree of pre-seismic increase during period B at the stations. (d) Spatial distribution of the degree of post-seismic decrease during period C at the stations. (e) Spatial distribution of the difference between the period B increase and period C decrease. The stations that were used by Heki and Enomoto [2013] are indicated by the larger circles with thick lines.

4-3. Propagation of the pre-seismic enhancement

Heki and Enomoto [2013] has already pointed out that a LSTID, which traveled at ~0.3 km/s from north to south and arrived at the source area ~1 h before the mainshock, can provide one potential explanation for the TEC enhancement before the Tohoku-Oki Earthquake. However, Heki and Enomoto [2015] showed that the appearance of the breaks within the latitude range of the ruptured fault area is simultaneous, and then suggested that the signatures of the breaks differ from that due to space weather. Figure 5a shows the arrival time distribution of the TEC breaks for satellite PRN15. The break is represented by the $-\Delta$AIC peak, which propagates from north to south, with a temporary acceleration seen around 04:50 UTC above the source region of the Tohoku-Oki Earthquake. This acceleration corresponds to the reported simultaneous enhancement. However, these accelerations/decelerations often occur during LSTID propagation, such that the LSTID propagation is not necessarily constant in velocity and direction. Figures 5b and 5c, and Movie S1 show the –ΔAIC propagation on the day of the Tohoku-Oki Earthquake (DOY70) and the previous day (DOY69). The positive/negative breaks change the propagation velocity, and frequently appear and disappear during the LSTID propagation, as their nature. For example, positive breaks appear simultaneously even on DOY69 (from 35 to 37°N around 05:40 UTC).

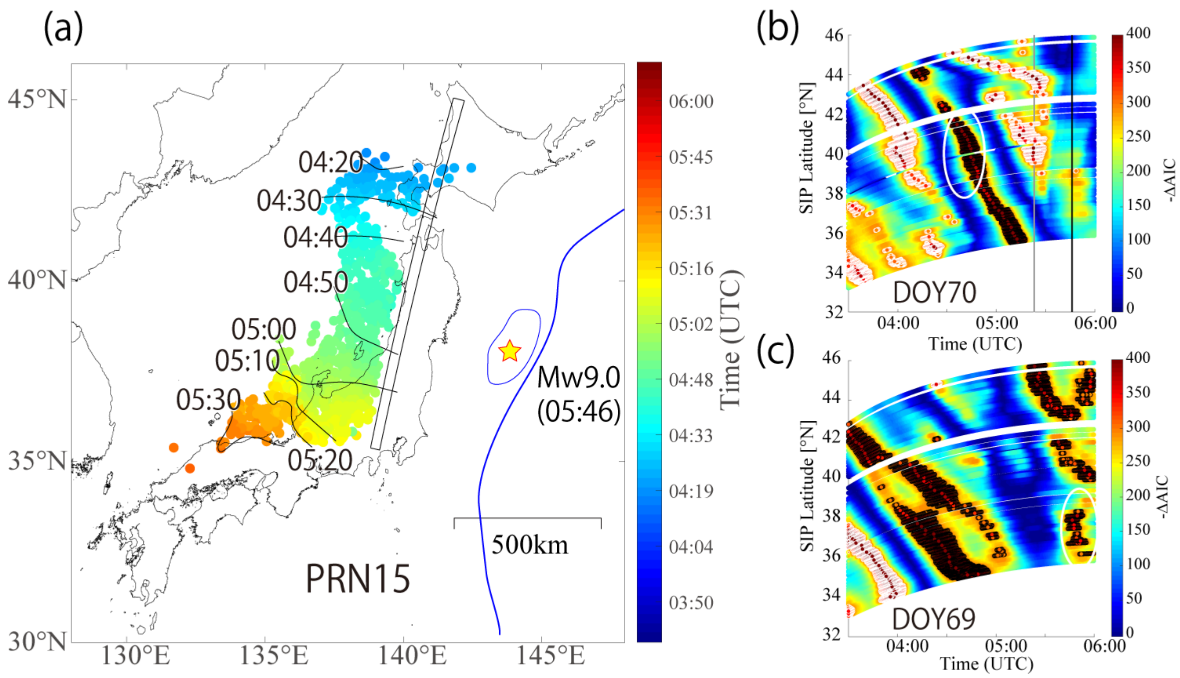

Figure 5. (a) Arrival time of the TEC break in the ±30-min window about the mainshock (05:46 UTC). The circles show the SIPs for satellite PRN15 at the time of the peak –ΔAIC value, whose slope is larger than the threshold (3.0 TECU/h and 75%), which represents the positive TEC break. The contours show the arrival time in 10-min intervals. The thick blue line marks the Japan Trench, and the star shows the epicenter of the 2011 Tohoku-Oki

Earthquake. The area enclosed by the thin blue line is the large-slip area (>10 m) that was determined by Ikuta et al. [2012]. The rectangle extending from 35 to 45°N shows the area of the selected stations that was used to depict the –ΔAIC propagation in Figures 5b and 5c. (b) –ΔAIC propagation among the selected stations for satellite PRN15 before the Tohoku-Oki Earthquake (05:46 UTC on DOY70). The circles with black and white edges indicate the positive and negative breaks, respectively, for –ΔAIC values larger than 300. The vertical black line marks the time of the mainshock. The vertical gray line denotes 05:23 UTC, which corresponds the start of the 30-min window, which includes the co-seismic disturbance (CID) starting at 05:53 UTC. The white ellipse around 04:40 UTC shows the acceleration of the LSTID propagation (a positive break), which Heki and Enomoto [2015] highlighted as a simultaneous appearance. (c) Same as Figure 5b, but for the previous day (DOY69). The white ellipse around 05:40 UTC shows the acceleration of the LSTID propagation (a positive break).

4-4. Spatiotemporal distribution of post-seismic VTEC depletion

A large post-seismic TEC depletion was observed around the source region at the time of the Tohoku-Oki Earthquake, as reported from observations (e.g., Saito et al., 2011; Kakinami et al., 2012) and numerical models [Shinagawa et al., 2013]. Here we analyze this post-seismic depletion from a spatiotemporal perspective.

We correct the inter-trace biases (ITBs) due to the ambiguity of the code pseudo range, as mentioned in the Appendix, to observe the faint spatial variations in the VTEC time series. Figure 6 shows the spatial distribution of the corrected VTECs for satellite PRN26, whose SIPs pass through the large-slip area around the time of the mainshock. A round-shaped hole is seen around the epicenter, even 54 min after the earthquake (Figures 6b and 6c).

The TEC values at the center of the depletion area are ~5 TECU less than those of the surrounding area. The diameter of the hole seems to expand with time (Figures 6b and 6c, and Figures 6e and 6f). Movie S2 shows the pre- and post-seismic TEC variations at a 30-s sampling interval. The movie indicates that the first significant co-seismic disturbance (CID) appears above the source area at 05:55 UTC for satellite PRN26, which is ~9 min after the mainshock. This CID propagation has been reported by many papers (e.g. Tsugawa et al. 2011; Astafeyva et al. 2011; Kakinami et al. 2012). At least four positive peaks, each with a different velocity, propagate from the source region to the southwest and to the north, with the amplitude of the first wave being especially large. A hole that is centered at the radiant point of the CID emerges at around 06:05 UTC, after these peaks propagated across the area. Four other satellites also show a post-seismic hole, even though its outline is not as sharp as that observed with satellite PRN26 (Movie S3). Movie S3 shows that post-seismic VTEC depletion is observed, even 120 min after the mainshock, and extends at least 500 km from the high-slip area for all of the satellites in view (PRN9, 15, 12, and 27). The spatial extent of the depletion area is not necessarily isotropic, but rather elongate in the northwest direction from the radiant point, which may reflect the alignment of the lifted area along the trench. He and Heki [2017] studied the pre-seismic TEC enhancement before M 7–8 earthquakes using the reference curves, and claimed that these depletions should be limited spatially above the focal area, even if post-seismic holes exist, such that excluding the approximately ±30-min window around the earthquake is enough to avoid these effects since the IPP passes through the area within this period. However, they must have considered the spatial extent of the post-seismic depletion more carefully when adopting the window of data to exclude, since the spatial extent of the depletion area is much larger than the focal area in the case of the Tohoku-Oki Earthquake.

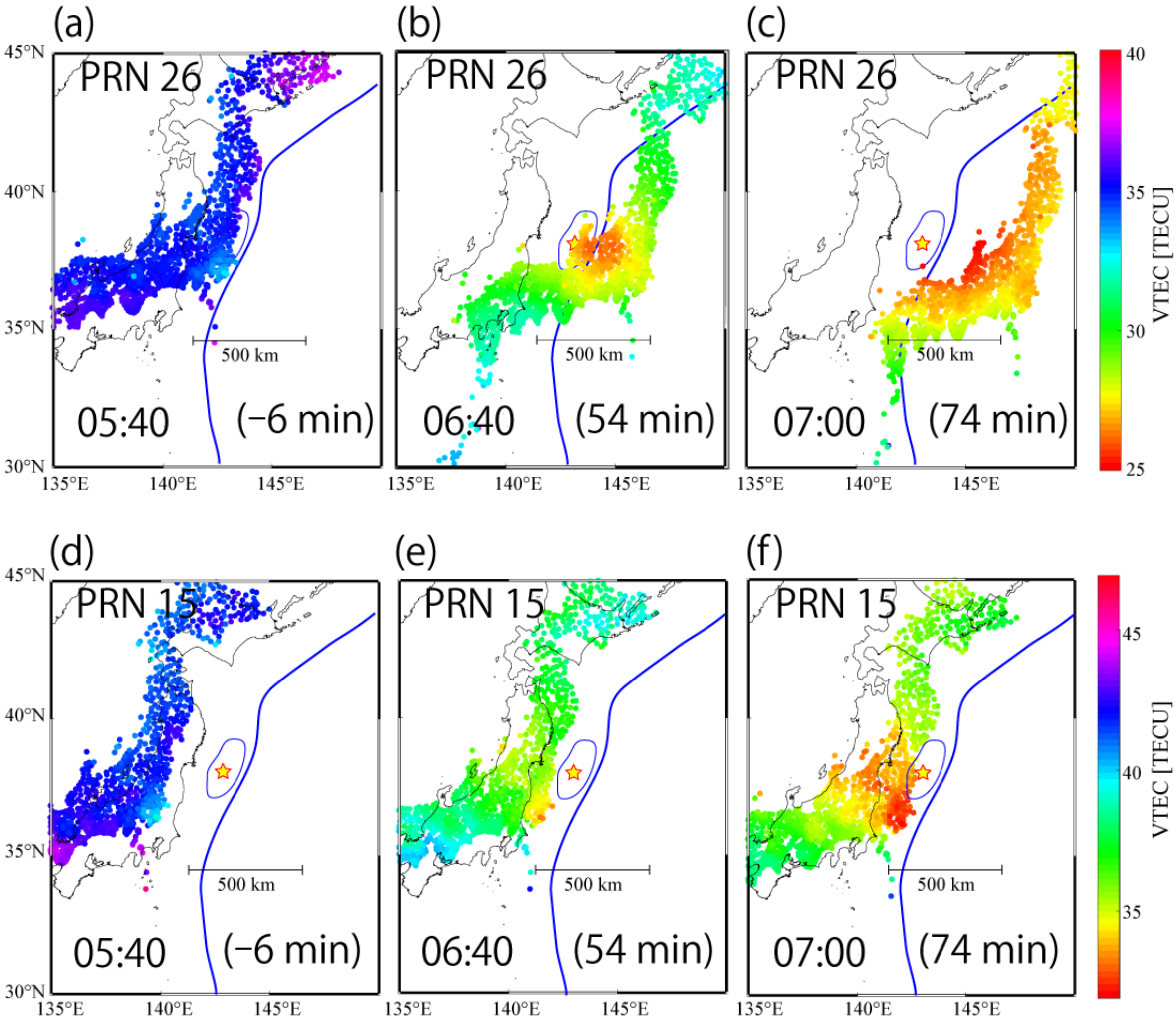

Figure 6. Absolute VTEC distribution. Satellite PRN26 at (a) 05:40, (b) 06:40, and (c) 07:00 UTC, and satellite PRN15 at (d) 05:40, (e) 06:40, and (f) 07:00 UTC on March 11, 2011. The dots are color-coded to show the absolute VTEC value for each IPP location at 300 km height. The thick blue line shows the Japan Trench, and the red star shows the epicenter of the 2011 Tohoku-Oki Earthquake. The area enclosed by the thin blue line is the large-slip area (>10 m) that was determined by Ikuta et al. [2012]. The times in parentheses indicate the lapse times relative to the mainshock.

5. Conclusion

We statistically evaluated the occurrence rate of the positive TEC breaks proposed by Heki and Enomoto [2015] using the same procedure and threshold as in their study. Our averaged occurrence rate of TEC enhancement is much larger than that reported by Heki and Enomoto [2015] since we used all of the visible GPS satellites at GNSS station 3009. We detected 198 positive breaks within the 305-h time period using a 25° elevation mask angle. There was a 62% probability of at least one positive break occurring within a given 90-min period. Therefore, we cannot rule out the possibility that the pre-seismic VTEC changes, detected using the same procedure and threshold within 90 min before the 2011 Tohoku-Oki Earthquake and the other four great earthquakes, are just a product of chance, as the space weather-related LSTID and instability of the observed VTEC are potential candidates for these pre-seismic VTEC changes. Post-seismic VTEC depletion lasted at least 2 h and extended more than 500 km from the epicenter of the 2011 Tohoku-Oki Earthquake. This suggests that we must consider the spatial extent of post-seismic TEC depletion carefully when we adopt a reference curve that excludes a time window to estimate VTEC enhancement.

Appendix

Inter-trace bias (ITB) correction

The TEC traces still show biases of up to a few TECU, even between adjacent stations, after correcting the DCBs and IFBs for the satellites and stations, respectively. An example of the VTEC distribution at a moment for PRN15 is shown in Figure A1a. A random variation up to a few TECU is seen in the residual distribution after the local spatial averages are subtracted from the VTEC. A pair of STEC traces with a common satellite will show almost constant bias during a period when the satellite is continuously visible.

We recognize these biases as ITBs, which should arise from uncertainties in the code pseudo range. The pseudo range has large variances up to a few TECU, as well as a drift bias that cannot be fit very well by the L4 shift (as described in section 2-1), even though the pseudo range is free of integer ambiguity. We therefore need to correct the ITB to study the faint spatial variation in TEC. We estimate the ITB based on the spatial average of the VTEC every hour. We define $VTEC_{ave\,ij}$ for the i-th station and the j-th satellite by the weighted average of the measured VTEC as follows:

$$VTEC_{pre\,ij}(t) = \frac{\sum_{m\neq i} VTEC_{mj}(t)\exp(-\frac{r_{mi}}{D})}{\sum_{m\neq i}\exp(-\frac{r_{mi}}{D})}, \quad (3)$$

where r is the horizontal distance from the SIP to the grid point at location (x, y) and D is the decay distance, which is set to 20 km. The summation is done for the stations within 60 km of the i-th station. One ITB is estimated for the trace of each satellite–station pair as the residual between the observed and predicted VTEC:

$$ITB_{ij} = \frac{1}{l}\sum_{n=1}^{l} \frac{\{VTEC_{ij}(t_n) - VTEC_{pre\,ij}(t_n)\}}{cos\psi_{ij}(t_n)}, \quad (4)$$

where l is the number of hours in the trace. To deduce the $VTEC_{pre\,ij}$, we select the stations that possess a residual of less than 3 TECU from $VTEC_{pre\,mj}$ for a robust estimation of $VTEC_{pre\,ij}$. We excluded 06:00 UTC during the ITB estimation to avoid the affect of the CID, which starts around 05:55. Each trace generally continues for 1–5 h. We finally obtain the corrected VTEC time series by subtracting $ITB_{ij}cos\psi_{ij}(t)$ from the initial VTEC time series.

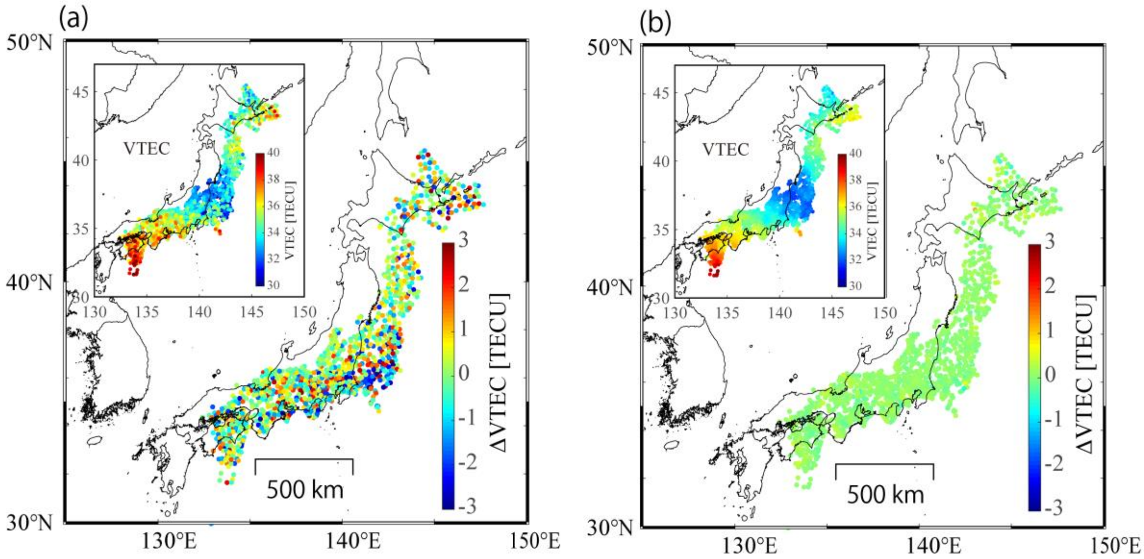

Figure A1. VTEC distribution before and after the correction with PRN15 satellite at 7:20UT (1h34m after the main shock). (a) VTEC residual from the local spatial average before the correction. The dots are color-coded to show the VTEC residual value for each IPP location at 300 km height. Imposed panel show the absolute VTEC. (b) Same with Figure A1a but after the correction. The color scale for the main and the imposed panels are common with that in Figure A1a.

Acknowledgements

All GPS data were downloaded from Geospatial Information Authority of Japan (https://terras.gsi.go.jp/). We acknowledge Dr. T. Sakai at the Electronic Navigation Research Institute (https://www.enri.go.jp/) and the University of Bern (ftp.unibe.ch) for providing the receiver IFBs and satellite DCBs, respectively. We also acknowledge K. Yamaoka and Y. Mitsui for improving this manuscript through insightful discussions.

References

Astafeyva, E., Lognonne P., & Rolland, L. (2011), First ionospheric images of the seismic fault slip on the example of the Tohoku-oki earthquake, *Geophys*. *Res*. *Lett*., 38, L22104.

Heki, K. (2011), Ionospheric electron enhancement preceding the 2011 Tohoku-Oki earthquake, *Geophys*. *Res*. *Lett*., 38, L17312.

Heki, K. & Enomoto, Y. (2013), Preseismic ionospheric electron enhancements revisited, *J. Geophys. Res., Space Physics*, 118, 6618–6626, doi:10.1002/jgra.50578.

Heki, K. & Enomoto, Y. (2015), M_w dependence of pre-seismic ionospheric electron enhancements, *J. Geophys. Res. Space Phys., 120*, 7006-7020.

He, L. & Heki, K. (2016), Three-dimensional distribution of ionospheric anomalies prior to three large earthquakes in Chile, *Geophys. Res. Lett., 43*, 7287-7293.

He, L. & Heki, K. (2017), Ionospheric anomalies immediately before M_w 7.0-8.0 earthquakes, *J. Geophys. Res. Space Phys.,122*, 8659–8678.

He, L. & Heki, K. (2018), Three-dimensional tomography of ionospheric anomalies immediately before the 2015 Illapel earthquake, central Chile, *J. Geophys. Res. Space Phys*., 123, 4015–4025. https://doi.org/10.1029/2017JA024871

Ikuta, R., Satomura, M., Shimada, S., Fujita, A. & Ando, M. (2012), A small persistent locked area associated with the 2011 Mw9.0 Tohoku-Oki earthquake, deduced from GPS data, *J*. *Geophys*. *Res*. *Solid Earth*, 117, B11408, doi:10.1029/2012JB009335

Kakinami, Y., Kamogawa, M., Tanioka, Y., Watanabe, S., Gusman, A. R., Liu J-Y., Watanabe, Y., & Mogi, T. (2012), Tsunamigenic ionospheric hole, *Geophys*. *Res*. *Lett*., 39, L00G27, doi:10.1029/2011GL050159.

Kamogawa, M. & Kakinami, Y. (2013), Is an ionospheric electron enhancement preceding the 2011 Tohoku-oki earthquake a precursor?, *J. Geophys. Res. Space Phys., 118*, 1-4, doi:10.1002/jgra.50118.

Masci, F., Thomas, J.N., Villani, F., Secan, J.A., & Rivera, N. (2015), On the onset of ionospheric precursors 40 min before strong earthquakes, *J. Geophys. Res. Space Physics*, 120, 1383–1393, doi:10.1002/2014JA020822.

Saito, A., Tsugawa, T., Otsuka, Y., Nishioka, M., Iyemori, T., Matsumura, M., Saito, S., Chen, C. H., Goi, Y. & Choosakul, N. (2011), Acoustic resonance and plasma depletion detected by GPS total electron content observation after the 2011 off the Pacific coast of Tohoku Earthquake, *Earth Planets Space*, 63, 863–867.

Sakai, T. (2005), Bias error calibration for observing ionosphere by GPS network, *J. Inst. Electron. Inf. Commun. Eng.*, J88-B, 2382–2389, (in Japanese).

Shinagawa, H., Tsugawa, T., Matsumura, M., Iyemori, T., Saito, A., Maruyama, T., Jin, H., Nishioka, M., & Otsuka, Y. (2013), Two-dimensional simulation of ionospheric variations in the vicinity of the epicenter of the Tohoku-oki earthquake on 11 March 2011, *Geophys. Res. Lett.*, 40, 5009–5013, doi:10.1002/2013GL057627.

Tsugawa, T., Saito, A., Otsuka, Y., Nishioka, M., Maruyama, T., Kato, H., Nagatsuma, T., & K. T. Murata (2011), Ionospheric disturbances detected by GPS total electron content observation after the 2011 off the Pacific coast of Tohoku Earthquake, *Earth Planets Space*, 63, 875–879.